1D, 2D, and 2D Parallel Interpenetrated Dicarboxylato Bridged Co(II) Metal Organic Frameworks: Synthesis, Crystal Structure, Fluorescence Sensing and Band Gap Calculation

Soumen Mistri,[a] Ennio Zangrando,[b] Pavel Vojtíšek,[c] and Subal Chandra Manna*[a]

Metal organic frameworks of Co(II), $\{[Co(bphz)_{1.5}(tp)(H_2O)_2]\cdot 3.2H_2O\}_n$ (**1**), $\{[Co(bphz)(ip)]\cdot(bphz)_{0.5}\}_n$ (**2**), and $[Co(bpp)(ppda)(H_2O)_2]_n$ (**3**) [where bphz = N,N′-bis-pyridin-4-ylmethylene-hydrazine; tp = 1,4-benzenedicarboxylate; ip = 1,3-benzenedicarboxylate; bpp = 1,3-bis(4-pyridyl)propane; ppda = 1,4-phenylenediacrylate] have been synthesized and characterized by single crystal X-ray diffraction and spectroscopic studies. Complex **1** is a ladder like 1D polymeric chain, **2** is a 2D porous sheet, while **3** is a 2D parallel interpenetrated network. The band gap of complexes has been calculated using solid state reflectance spectra, and results show that complexes act as semiconductor. In dispersed methanolic solution complexes **1–3** exhibit intense fluorescence at room temperature. The complexes were tested with several aromatic compounds such as benzene, nitrobenzene, *o*-nitrotoluene and *p*-nitrotoluene, etc., in dispersed methanol medium. Results show that complex **3** selectively senses nitro aromatic compounds and this behavior has been explained on the basis of PET and RET mechanisms.

Introduction

During the last two decades, research on metal-organic frameworks (MOFs) built with 3d transition elements and organic bridging ligands has been of great interest due to the intriguing structural diversity of the compounds obtained[1] and their potential application as functional materials in the area of catalysis, porosity, magnetism, luminescence, conductivity, sensing, nonlinear optics and chirality.[2–7] These compounds present structure and properties that depend on several factors such as reaction conditions,[8] metal ion, organic ligands,[9] solvent,[10] metal-ligand ratio[11] and weak interactions.[12] Among the several factors, suitable choice of ligands and of metal ions is crucial for tuning the conformational/structural dimension of MOFs.[13] Literature survey reveals that various architectures e. g. diamondoid,[14] honey comb,[15] grid,[16] T-shaped,[17] ladder,[18] brick wall,[16a,18a] and parallel/inclined interpenetrated[10a,13,19,20] have been reported by proper combination of organic ligands and metal ions. Long organic ligands [rigid/flexible] often yield interpenetrated structures and a large number of interpenetrated structures, ranging from two-up to ten-fold, has been reported.[21]

Combination of rigid aromatic dicarboxylates with rigid/flexible long spacer is a common strategy for designing MOFs of high dimension, where carboxylates have the double function to bridge the metal ions and partially or fully counterbalance their charge. On the other hand neutral spacers enhance the dimensionality of the compounds. In the literature several multidimensional MOFs with interesting structures are reported using nitrogen/oxygen donor neutral ligands in combination with aromatic dicarboxylates.[22,23] Among the latter, p-phenylenediacrylic (H_2ppda),[13] terephthalic (H_2tp)[10a,20a] and isophthalic acid (H_2ip),[24] are members of multidentate aromatic dicarboxylic acids having carboxylic groups orientated at 180°or 120°, and are potential for designing Co(II) based MOFs. Using terephthalate a number of 2D inclined and parallel interpenetrated networks, such as $\{[Co(bpe)(tp)(H_2O)_2]\cdot 2.5H_2O\}_n$,[10a] and $\{[Co(bpe)(tp)(H_2O)_2]\cdot(glycol)\}_n$,[10a] beside 1D MOFs, $\{[Co(dpyo)(tp)(H_2O)_2]\cdot[Co(H_2O)_6]\cdot(tp)\cdot H_2O\}_n$,[25] and $[Co(bpp)(tp)(H_2O)_2]$[20a] has been reported. Using p-phenylenediacrylate recently our group reported a 1D polymeric chain $\{[Co(ppda)(dpyo)(H_2O)_3]\cdot 4H_2O\}_n$[13] and a 3-fold interpenetrated α-polonium network $\{[Co(ppda)(bpe)]\cdot 0.5H_2O\}_n$.[13]

Fluorescence quenching based detection of ultra trace-analytes is a central challenge in the area of chemical sensors,[26] and recently carboxylato bridged MOFs showing selective fluorescence sensors for aromatic compounds have been reported.[27]

In this contribution we report 1D ladder, 2D porous and 2D parallel interpenetrated MOFs of cobalt using aromatic dicar-

[a] *Dr. S. Mistri, Dr. S. C. Manna*
Department of Chemistry and Chemical Technology
Vidyasagar University
Midnapore 721102, West Bengal, India
Fax: (91) (03222) 275329
Web:
E-mail: scmanna@mail.vidyasagar.ac.in
Homepage: http://vidyasagar.ac.in/Faculty/Profile?fac_u_id = Fac-CHEM-8
[b] *Prof. E. Zangrando*
Department of Chemical and Pharmaceutical Sciences
University of Trieste
34127 Trieste, Italy
[c] *Prof. P. Vojtíšek*
Department of Inorganic Chemistry
Charles University in Prague
Hlavova 2030/8, 128 43 Prague 2, Czech Republic

Supporting information for this article is available on the WWW under http://dx.doi.org/10.1002/slct.201700237

boxylates and N donor rigid/flexible long spacers. Combination of linear tp with rigid spacers bphz results in a ladder like 1D polymeric compound {[Co(bphz)$_{1.5}$(tp)(H$_2$O)$_2$]·3.2H$_2$O}$_n$ (**1**). When combination of angular ip and rigid bphz are used, a 2D porous compound {[Co(bphz)(ip)]·(bphz)$_{0.5}$}$_n$ (**2**) is formed. On the other hand combination of relatively longer linear carboxylate (ppda) with flexible spacer bpp results in 2D parallel interpenetrated compound [Co(bpp)(ppda)(H$_2$O)$_2$]$_n$ (**3**). Complexes **1–3** are fluorescent when dispersed in methanol. The effect of various aromatic compounds on the fluorescence of complexes **1–3** has been investigated. For all compounds a great fluorescence quenching is observed in presence of electron deficient aromatic compounds. The determination of optical band gaps for the metal complexes, evaluated by diffuse-reflectance UV-vis spectra, show that **1–3** may function like semiconductor.

Results and Discussion

IR Spectral Studies

IR spectra of complexes **1–3**, free pyridyl ligands, and sodium salt of carboxylates are shown in Figures 1S-8S and the more significant bands are summarized in Table 1S. Complexes **1** and **3** exhibit broad bands in the region 3100 −3600 cm^{-1}, which are assigned to be ν(O-H) stretching vibrations of water molecules.[28a] The weak bands in the region 2982–2989 cm^{-1} correspond to aromatic ν(C–H) stretching vibrations in **1–3**, and imine C_{sp2}-H stretching vibration in **1** and **2.** The band at 2946 cm^{-1} for **3** is due to aliphatic C_{sp3}-H stretching vibration of bpp ligand. ν_{as}(OCO) stretching vibrations for **1** and **3** appear at 1647 cm^{-1} and 1644 cm^{-1}, respectively; whereas for **2**, ν_{as}(OCO) stretching vibrations appear at 1572 and 1555 cm^{-1}. For both **1** and **3**, ν_s(OCO) stretching vibration falls at 1374 cm^{-1}, on the other hand for **2**, ν_s(OCO) stretching vibrations appear at 1470 and 1417 cm^{-1}. To get better understanding about the carboxylate stretching of complexes, we have compared IR spectral results of complexes with IR spectral results of sodium salts of respective carboxylates. The comparisons are given in Tables 1S and 2S. Very high separation of stretching frequencies, Δν [$\Delta\nu = \nu_{as}$(OCO) - ν_s(OCO); 273 cm^{-1} for **1,** and 270 cm^{-1} for **3**], corroborates the presence of monodentate coordination mode of carboxylates in **1** and **3.** Low (85 cm^{-1}) and moderate (155 cm^{-1}) Δν values for **2** correspond to the bidentate chelating and bidentate bridging coordination, respectively. These are also further illustrated by comparison of Δν values for complexes and for sodium salt of carboxylates. Generally observed trends are $\Delta\nu_{\text{studied complex}} \gg \Delta\nu_{\text{sodium salt}}$, $\Delta\nu_{\text{studied complex}} \leq \Delta\nu_{\text{sodium salt}}$ and $\Delta\nu_{\text{studied complex}} \ll \Delta\nu_{\text{sodium salt}}$, for monodentate carboxylate, bidentate bridging carboxylate and bidentate chelating carboxylate, respectively.[28] In the present study $\Delta\nu_{(\text{complex 1})}$ (273 cm^{-1}) and $\Delta\nu_{(\text{complex 3})}$ (270 cm^{-1}) $> \Delta\nu_{\text{sodium salt}}$ (for both Na$_2$tp and Na$_2$ppda, 227 cm^{-1}), and $\Delta\nu_{(\text{complex 2})}$ (155 cm^{-1} and 85 cm^{-1}) $\ll \Delta\nu_{\text{sodium salt}}$ (for Na$_2$ip 244 cm^{-1}). All these observations corroborate crystallographically characterized (*vide infra*) coordination modes carboxylates in complexes **1–3.** The bands in the region 1466–1572 cm^{-1} correspond to ν(C=C) and ν(C=N) stretching vibrations in **1–3.** ρ_r(H$_2$O) bands of compounds **1** and **3** appear at 819 cm^{-1}. Weak bands of **1** and **3** in the region 658–644 cm^{-1} correspond to ρ_w(H$_2$O). The presence of ρ_r(H$_2$O) and ρ_w(H$_2$O) bending vibrational modes indicate the presence of coordinated water molecules in **1** and **3.**

Crystal Structure Description

Single-crystal X-ray analyses show that the conformations and the functions of the ligands play an important role in affecting the final structural motifs of the polymers obtained. The self-assembly process of Co(II) salt with 1,2-bis(4-pyridylmethylene) hydrazine and terephthalate anion, acting as di-topic subunits, results in a 1D coordination polymer (**1**), while changing the anion with isophthalate a 2D framework (**2**), containing dicobalt Co_2 units, is obtained. A novel parallel interpenetrated 2D structure (**3**) of (4,4) topology is obtained with the more flexible neutral 1,3-bis(4-pyridyl)propane spacer in connection with 1,4-phenylenediacrylic acid.

{[Co(bphz)$_{1.5}$(tp)(H$_2$O)$_2$]·3.2H$_2$O}$_n$ (1)

Single-crystal X-ray analysis reveals that **1** is a one-dimensional coordination polymer. Each Co^{II} center has a slightly distorted {N$_2$O$_4$} octahedral chromophore (the ORTEP drawing of the coordination sphere is depicted in Figure 9S). Two nitrogen donors are located in *trans* positions of the octahedron, one comes from a monodentate, the other from a bridging bphz connector. The four oxygen donors in the equatorial plane derive from two aqua ligands and two carboxylate groups from a terephthalate anion acting as bridging bis-monodentate ligand. The Co–O(carboxylate) bond lengths, of 2.0670(13) and 2.0486(13) Å, appear slightly shorter than the Co-O(water) and Co–N bond lengths that range from 2.1357(15) to 2.1739(16) Å. The carboxylate groups are coplanar with the central aromatic ring, as well as the pyridine rings of the bridging bphz, being located on a center of symmetry. On the other hand the pyridine rings of the monocoordinated bphz form a dihedral angle of 13.5°. The relative coordination bond angles reported in Table 1 indicate small distortions from the ideal octahedral geometry. Intrachain hydrogen bonds around the coordination sphere reinforce the overall structure [O(1w)–O(4) = 2.624(2); O(2w)–O(2) = 2.659(2) Å] (Figure 9S). The structural analysis evidences a polymeric arrangement with a ladder-like motif in which two [Co(H$_2$O)$_2$(tp)]$_n$ chains are linked by bphz species that feature the rungs (Figure 1).

Thus the framework appears to be composed of parallelogram boxes, of dimensions 11.385 × 15.744 Å, corresponding to the Co–Co separation across the tp and bphz, respectively. The polymer is bordered by monodentate bphz ligands that complete the metal coordination sphere (Figure 1). The water molecules (two of these at low occupancy, see experimental Section) dispersed in between the polymeric chains lead to a 3D network through a H-bonding scheme (Figure 2).

In particular O(3w) and O(5w) interacts with the uncoordinated nitrogen of the pendant bphz, and in turn with another lattice water molecule O(4w). The geometrical data relative to

Table 1. Coordination bond lengths [Å] and angles [°] for complexes **1–3.**

Complex 1			
Co-N(1)	2.1435(16)	Co-O(3)	2.0486(13)
Co-N(5)	2.1739(16)	Co-O(1w)	2.1627(15)
Co-O(1)	2.0670(13)	Co-O(2w)	2.1357(15)
O(3)-Co-O(1)	176.85(6)	O(2w)-Co-O(1w)	178.52(5)
O(3)-Co-O(2w)	90.00(6)	N(1)-Co-O(1w)	87.60(6)
O(1)-Co-O(2w)	93.16(6)	O(3)-Co-N(5)	90.83(6)
O(3)-Co-N(1)	88.81(6)	O(1)-Co-N(5)	89.47(6)
O(1)-Co-N(1)	90.96(6)	O(2w)-Co-N(5)	87.29(6)
O(2w)-Co-N(1)	91.51(6)	N(1)-Co-N(5)	178.74(7)
O(3)-Co-O(1w)	91.16(6)	O(1w)-Co-N(5)	93.61(6)
O(1)-Co-O(1w)	85.68(5)		
Complex 2			
Co-N(1)	2.1583(16)	Co-O(2)	2.1915(14)
Co-N(4‴)	2.1393(16)	Co-O(3″)	2.0420(12)
Co-O(1)	2.1549(13)	Co-O(4′)	2.0178(14)
O(4′)-Co-O(3″)	116.32(5)	N(4‴)-Co-N(1)	177.34(6)
O(4′)-Co-N(4‴)	90.98(6)	O(1)-Co-N(1)	91.86(6)
O(3″)-Co-N(4‴)	92.44(6)	O(4′)-Co-O(2)	149.75(5)
O(4′)-Co-O(1)	90.06(5)	O(3″)-Co-O(2)	93.13(5)
O(3″)-Co-O(1)	153.48(6)	N(4‴)-Co-O(2)	94.66(6)
N(4‴)-Co-O(1)	89.55(6)	O(1)-Co-O(2)	60.35(5)
O(4′)-Co-N(1)	86.75(6)	N(1)-Co-O(2)	88.00(6)
O(3″)-Co-N(1)	87.31(6)		
Complex 3			
Co-N(1)	2.1477(15)	Co-O(2′)	2.0908(12)
Co-N(2″)	2.1616(15)	Co-O(1w)	2.1218(13)
Co-O(1)	2.1226(12)	Co-O(2w)	2.1344(13)
O(1)-Co-N(1)	170.70(5)	N(1)-Co-N(2″)	85.90(6)
O(1)-Co-N(2″)	94.24(5)	O(1w)-Co-O(1)	84.27(5)
O(1)-Co-O(2w)	91.33(5)	O(1w)-Co-N(1)	86.52(5)
O(2′)-Co-O(1)	87.51(5)	O(1w)-Co-N(2″)	98.70(5)
O(2′)-Co-N(1)	94.00(5)	O(1w)-Co-O(2w)	174.63(5)
O(2′)-Co-N(2″)	169.77(5)	O(2w)-Co-N(1)	97.94(6)
O(2′)-Co-O(1w)	91.49(5)	O(2w)-Co-N(2″)	84.66(5)
O(2′)-Co-O(2w)	85.23(5)		

Symmetry codes for **2:** (′) -x+1, -y+1, -z+1; (″) x, y+1, z; (‴) x, y, z-1; for **3:** (′) -x+3/2, y+1/2, -z+3/2; (″) -x+1/2, y-1/2, -z+1/2.

the H-bonds are reported in Table 3S. The presence of these water molecules blocking a N donor at one bphz likely impedes the formation of a 2D net as observed for the close related structure {[Co(bpe)(tp)$(H_2O)_2]_n$ [bpe = 1,2-bis(4-pyridyl)ethane][10a] where the bpe behaves as a bridging ligand. Two isostructural structures of compound **1**, specifically one of nickel and the second of cobalt with a different amount of solvent, namely one CH_3OH and 1.5 water molecules, have been already reported.[10c]

{[Co(bphz)(ip)]·$(bphz)_{0.5}$}$_n$ (2)

When the terephthalate anion was replaced by its isomer, 1,3-benzenedicarboxylate, we obtained compound **2** of composition $[Co(bphz)(ip)]_n$, which exhibits a 2D layer of rectangular meshes, where dinuclear cobalt entities are located at the nodes and pair of neutral bphz ligands and pair of ip anions form the edges (Figure 3).

This is allowed by the different coordination mode of the ip carboxylate groups, one acting as bridging featuring the dinuclear entity, the other chelating towards another metal ion of a symmetry related

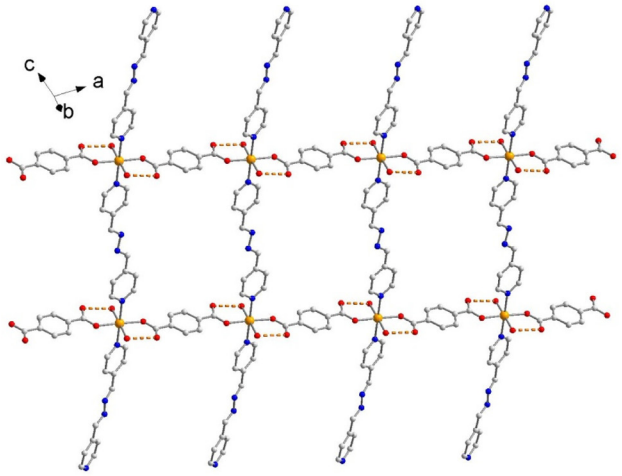

Figure 1. Schematic drawing of the ladder-like polymer of complex **1.**

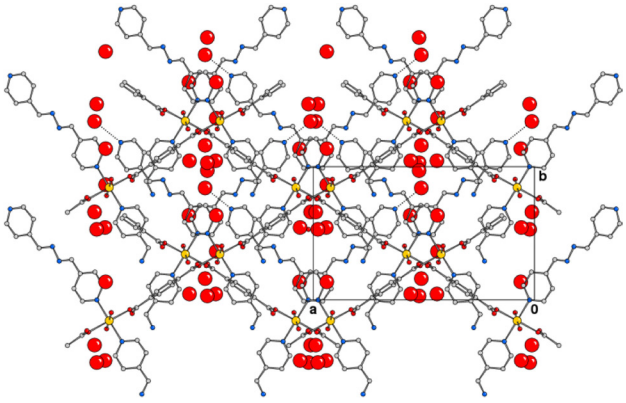

Figure 2. Crystal packing of compound **1** with indication of lattice water molecules (big spheres).

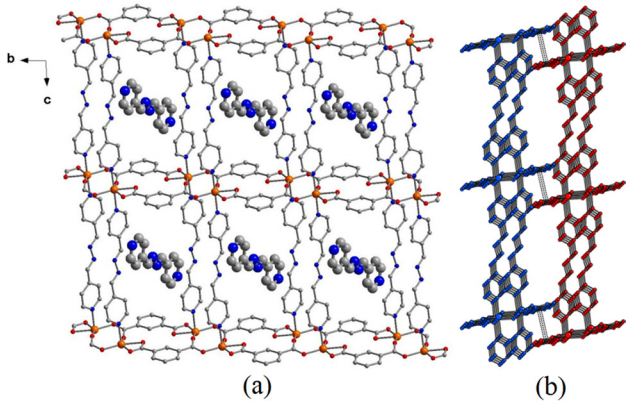

Figure 3. (a) 2D coordination polymer of compound **2** with lattice bphz molecules indicated as big spheres and (b) crystal packing down axis *c* showing two adjacent 2D networks (uncoordinated bphz molecules removed for clarity).

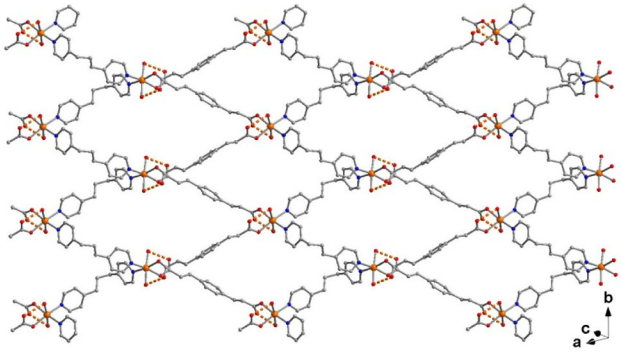

Figure 4. View of the 2D coordination polymer of compound **3** built by the 1,4-phenylenediacrylate anions and 1,3-bis(4-pyridyl)propane ligands.

pair. Thus two metals separated by 4.127 Å are bridged by two carboxylate groups in a centro-symmetric fashion, forming an octa-membered ring. Each cobalt(II) center completes the slightly distorted octahedral geometry with *trans* located bphz nitrogen donors, and the chelating carboxylate of another anion (Figure 10S). The Co–O coordination bond lengths of the chelating carboxylate group [Co-O(1) = 2.1549(13), Co-O(2) = 2.1915(14) Å] are slightly longer with respect to those involving the bridging carboxylate oxygen donors [2.0420(12) and 2.0178(14) Å]. The axial Co–N bond lengths are of 2.1583 (16) and 2.1393(16) Å fixing the N1-Co–N4 bond angle at 177.34(6)° (Table 1). The rectangular spaces defined by the bridging ligands are filled by the uncoordinated bphz molecules (Figure 3a) and suggest that the network can potentially behave as porous system. In fact the area left by these molecules account for 34.0% [422.2 $Å^3$] of the unit cell. Adjacent 2D layered networks are inter-digitated in the crystal packing as shown in Figure 3b connecting via π···π interactions realized between the isophthalate aromatic rings [centroid-to-centroid distance of 3.848(1) Å]. The uncoordinated bphz molecules, which show a high thermal motion, form a weak π interaction with N(1) pyridine ring of the framework [centroid-to-centroid distance of 4.330(2) Å]. Truly speaking during these studies the structure of **2** was reported by Bhattacharya *et al.*[24b]

$[Co(bpp)(ppda)(H_2O)_2]_n$ (3)

The X-ray structural analysis shows that compound **3**, of composition $[Co(bpp)(ppda)(H_2O)_2]_n$, consists of 2D corrugated layers of deltoid meshes (Figure 4), that is of kite-like shape having two pairs of adjacent sides of equal-length.

The edge formed by the bridging bpp ligands and the ppda anions space the metal ions at 12.530 and 15.320 Å, respectively. The nodes are occupied by cobalt ions exhibiting octahedral coordination geometry with a pair of bpp N donors and two ppda carboxylate O atoms *cis* located. The metal completes the coordination geometry with two aqua ligands at axial positions (Figure 11S). The pair of Co–N bond distances of 2.1477(15) and 2.1616(15) Å and the Co-OH_2 ones [2.1218(13) and 2.1344(13) Å] appear comparable in length, while the Co–O distances of the carboxylate oxygen atoms are slightly different of 2.1226(12) and 2.0908(12) Å. A careful analysis of the crystal structure shows parallel interpenetrated layers[29] (illustrated in Figure 5), which are formed by the long spacers but facilitated also by the conformation assumed by the bpp linker.

In fact this ligand exhibits a *TG (trans-gauche)* conformation[30] with torsion angles of 174.22(16) and 64.4(2)° about the propyl chain. Within the phenylenediacrylate anion the carboxylate groups form dihedral angles of 49.25 and 51.02° with the central ring likely in order to favor the interpenetration. The water molecules reinforce the whole structure being involved in intra-layer hydrogen bonds with carboxylate oxygens in the cobalt coordination geometry [O(1w)–O(4)′ and O(2w)–O(3) = 2.698(2) Å, Figure 11S], but also with those of the symmetry related interpenetrated layer [O(1w)–O(1) = 2.774(2) and O(2w)–O(2) = 2.782(2) Å], thus connecting the two 2D networks, as shown in Figure 5b.

It is worth of note that a unique complex having the same ligands was built with nickel(II) ions, $[Ni_5(ppda)_5(bpp)_5]\cdot 12H_2O$,[13b] having a parallel 2-fold interpenetrated layered structure (2D → 2D). However between the nickel derivative and complex **3** a different architecture is observed which is dictated by the different coordination mode of the dicarboxylate anions (bis-chelating and bis-monodentate, respectively), slightly different conformation of bpp, the presence of water molecules in the coordination sphere of **3.** These features determine a different shape of the windows and a different thickness of the layers (ca. 10 Å in the nickel complex and ca. 4 Å in compound **3**). Thus the water appear to have a template effect leading in both cases to interpenetrated 2D structures but of different topology.

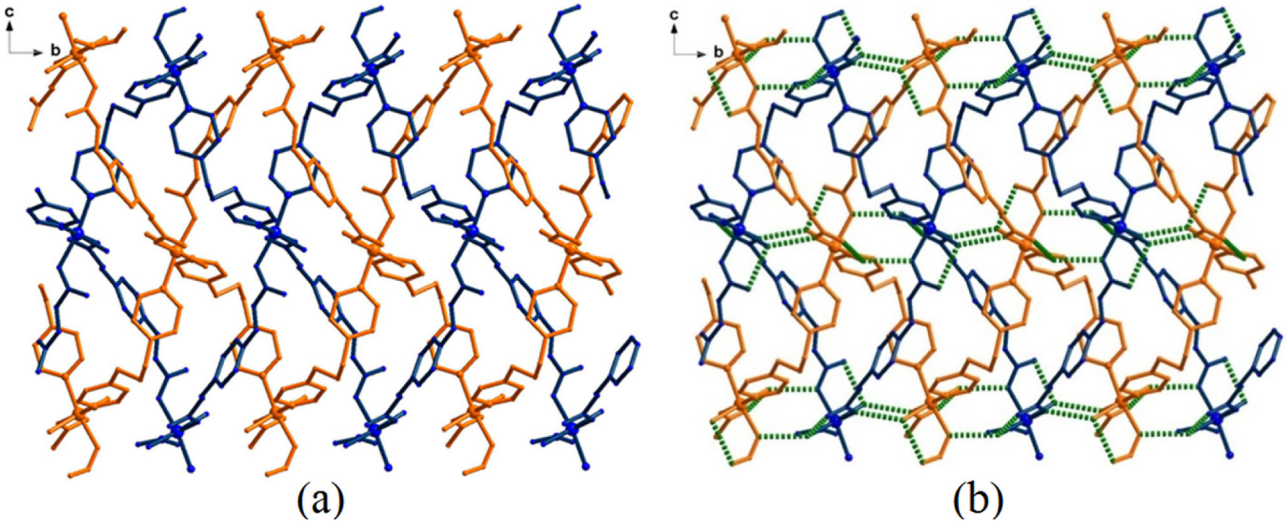

Figure 5. (a) 2D parallel interpenetrated nets viewed down axis *a* of compound **3.** (b) intra- and interlayer H bonds (dotted lines) involving water molecules and carboxylate oxygen atoms..

Table 2. Solid state electronic spectral data of complexes **1–3.**

Complex	$^4T_{1g}(F)\rightarrow{}^4T_{2g}(F)$ ν_1, cm^{-1}; (λ_1, nm)	$^4T_{1g}(F)\rightarrow{}^4A_{2g}(F)$ ν_2, cm^{-1}; (λ_2, nm)	$^4T_{1g}(F)\rightarrow{}^4T_{1g}(P)$ ν_3, cm^{-1}; (λ_3, nm)	ν_2/ν_1	10Dq (cm^{-1})	B (cm^{-1})
1	9049 (1105)	15748 (635)	19685 (508)	1.74	6699	1044
2	9689 (1032)	15197 (658)	19960 (501)	1.56	5508	1110
3	8795 (1137)	15873 (630)	19841 (504)	1.80	7078	1039

Solid State Electronic Spectra and Band Gap Calculation

Solid state UV-vis-NIR spectra of all the MOFs have been recorded and the data were collected in Table 2.

Figure 6 indicates that all the complexes exhibit d-d electronic transitions. The broad band in the region 9689–8795 cm^{-1} can be assigned to the spin allowed d-d transition $^4T_{1g}(F)\rightarrow{}^4T_{2g}(F)$ [$\bar{\nu}$, 9049 cm^{-1}; λ, 1105 nm for **1**; $\bar{\nu}$, 9689 cm^{-1}; λ, 1032 nm for **2**; $\bar{\nu}$, 8795 cm^{-1}; λ, 1137 nm for **3**]. The bands at $\bar{\nu}$, 19685 cm^{-1}; λ, 508 nm for **1**; $\bar{\nu}$, 19960 cm^{-1}; λ, 501 nm for **2**; and $\bar{\nu}$, 19841 cm^{-1}; λ, 504 nm for **3**, are characterized as spin allowed $^4T_{1g}(F)\rightarrow{}^4T_{1g}(P)$ transition. In addition to these bands the hump that appears at $\bar{\nu}$, 15748 cm^{-1}; λ, 635 nm for **1**; $\bar{\nu}$, 15197 cm^{-1}; λ, 658 nm for **2** and $\bar{\nu}$, 15873 cm^{-1}; λ, 630 nm for **3**, can be assigned as a $^4T_{1g}(F)\rightarrow{}^4A_{2g}(F)$ transition. From the Orgel diagram (ignoring configuration interaction), for weak field octahedral cobalt(II) (d^7) compounds $\overline{\nu_1}=8Dq$, $\overline{\nu_2}=18$ Dq and $\overline{\nu_3}=6Dq+15B$. These relations allow calculating the 10Dq values for complexes **1–3** of 6699, 5508 and 7078 cm^{-1}, respectively, which indicate higher ligand field strength in **3** as compared to that in **1** and **2.** The calculated B values are 1044, 1110 and 1039 cm^{-1} for **1**, **2** and **3**, respectively. Apart from d-d transitions, all the complexes show very higher energy transitions below 500 nm [325, 310 and 275 nm for **1**; 375 and 300 nm for **2**; and a broad band 200–400 nm for **3**]. These transitions correspond to intra-ligand charge transfer transitions.[31]

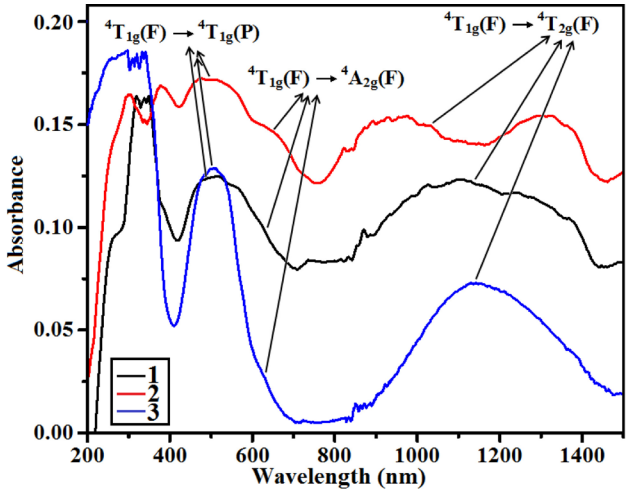

Figure 6. Solid state electronic spectra of complexes **1–3.**

The solid state reflectance spectra of MOFs help to calculate their band gaps. From Kubelka-Munk[32a] plot, the band gaps were calculated and for this plot the following equation was used

$$\alpha h\nu = A\ (E_{BG} - h\nu)^n \quad (1)$$

where α is the absorption coefficient, h Plank's constant, ν the frequency, A is a constant, n = 0.5 for direct allowed transition and n = 2 for indirect allowed transition, and E_{BG} is the band gap, calculated when $\alpha = 0$. The intersection point between the energy axis and the extrapolated line portion of the plot Kubelka-Munk function, $((\alpha h\nu)^{1/n})$ versus energy ($h\nu$), provides the E_{BG} band gap.[32] $(\alpha h\nu)^{1/n}$ *vs* $h\nu$ plot for compounds **1–3** is shown in Figure 7 [n = 2].

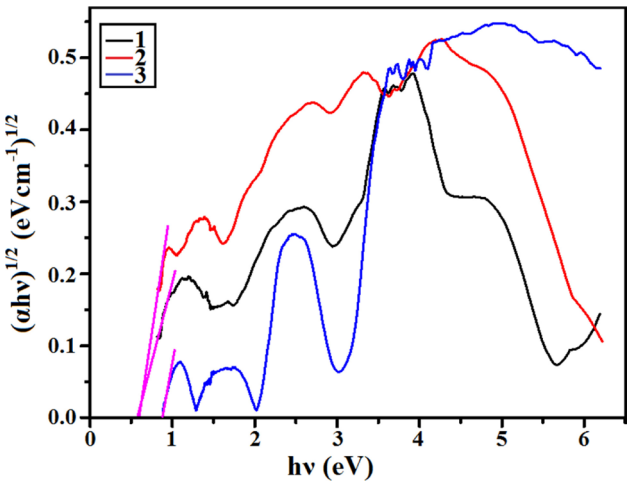

Figure 7. The diffuse reflectance UV-vis-NIR spectra of the $(\alpha h\nu)^{1/n}$ vs. energy (eV) of compounds **1–3** [n = 2].

Calculated values of band gaps are 0.52, 0.54 and 0.88 eV for **1**, **2** and **3**, respectively. These values indicate that all compounds may behave as semiconductor and, among them complex **3** may has less conducting ability compared to complexes **1** and **2.**

UV-vis Absorption Spectra and Effect of Benzene and its Derivatives

The UV-vis spectra of dispersed methanolic solution of **1–3** were recorded at room temperature. These spectra show different absorption bands with maxima at 277, 286, 298 and 310 nm for **1**; 282 nm for **2**; 213, 227, 233, 255, 262 and 313 nm for **3** (Figures 12S-14S). In order to investigate the sensing ability of **1–3**, we added 3 μL 5.079 mM methanolic solution of benzene (BN) and of its various derivatives such as toluene (TN), *o*-xylene (*o*-XY), *p*-xylene (*p*-XY), chlorobenzene (CB), bromobenzene (BB), nitrobenzene (NB), *o*-nitro toluene (*o*-NT) and *p*-nitro toluene (*p*-NT), to the 2.5 ml stock dispersed methanolic solution of MOFs. It is interesting to observe that a red shift with remarkable increasing of absorbance of the band in the region 275–282 nm [275 nm for **1**; 282 nm for **2**; 278 nm for **3**] takes place only in the presence of nitro derivatives of benzene, while in presence of benzene and other derivatives the band positions of MOFs remain same, although a change in absorbance is observed (Figures 12S-14S). Figures 15S and 16S show the change of absorption spectra upon gradual addition of nitrobenzene (3 μL 0.304 mM methanolic solution) to the 2.5 ml stock dispersed methanolic solution of **1** and **2**, respectively, and Figure 17S exhibits the UV-vis spectral change of **3** upon gradual addition of 3 μL 0.304 mM methanolic solution of *o*-nitrotoluene.

Fluorescence Property and Effect of Benzene and its Derivatives

All the complexes exhibit fluorescence in methanolic dispersed medium (Figure 8) (λ_{ex} = 286 nm, λ_{em} = 309, 331, 344 nm for **1**;

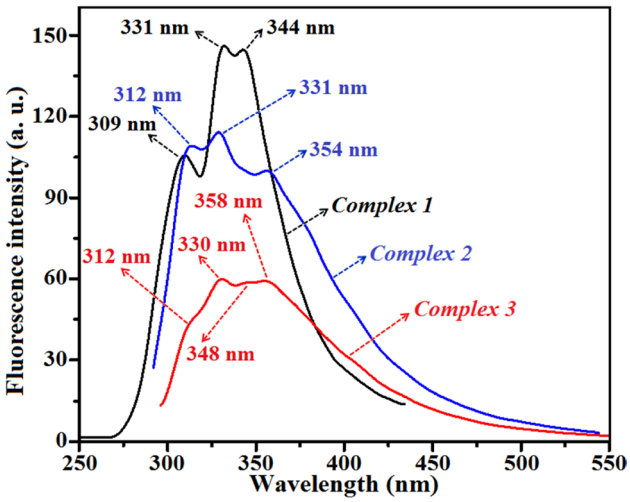

Figure 8. Fluorescence spectra of dispersed solution of complexes **1–3** in methanol at room temperature (λ_{ex} = 286 nm, λ_{em} = 309 nm, 331 nm, 344 nm for **1**; λ_{ex} = 282 nm, λ_{em} = 312 nm, 331 nm, 354 nm for **2** and λ_{ex} = 227 nm, λ_{em} = 312 nm, 330 nm, 348 nm for **3**).

λ_{ex} = 282 nm, λ_{em} = 312, 331, 354 nm for **2**; and λ_{ex} = 227 nm, λ_{em} = 312, 330, 348 nm for **3**). These are probably due to π-π^* transitions of organic ligands (bphz/bpp).[33]

In order to investigate the effect of benzene (BN) and its derivatives like toluene (TN), *o*-xylene (*o*-XY), *p*-xylene (*p*-XY), chlorobenzene (CB), bromobenzene (BB), nitrobenzene (NB), *o*-nitro toluene (*o*-NT) and *p*-nitro toluene (*p*-NT), on the emission behavior of different MOFs, we have added 3 μL 5.079 mM methanolic solution of different analytes to 2.5 ml dispersed methanolic solution of the MOFs.

Quenching of fluorescence intensities of all complexes was observed in presence of benzene, toluene, *o*-xylene, *p*-xylene, nitrobenzene, *o*-nitro toluene and *p*-nitro toluene, whereas enhancements of fluorescence intensities of all complexes were observed in presence of chlorobenzene and bromobenzene (Figures 9, 18S, and 19S). From Figure 10, it is clear that complexes **1** and **2** do not exhibit fluorescence selectivity for organic analytes. On the other hand complex **3** shows selective fluorescence quenching in presence of nitro aromatic compounds (NACs) and calculated fluorescence quenching efficien-

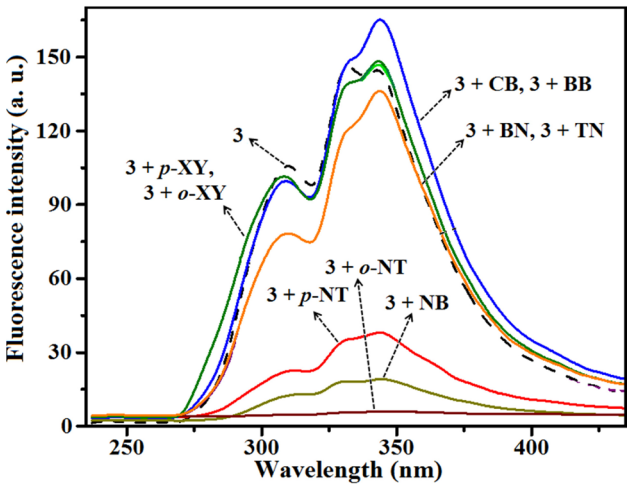

Figure 9. Fluorescence spectral changes of complex **3** (2.5 ml dispersed methanolic solution) upon addition of methanolic solution of benzene and its derivatives (3 μL 5.079 mM) at room temperature (λ_{ex} = 282 nm, λ_{em} = 312 nm, 330 nm, 348 nm, excitation and emission slit width = 2.5 nm).

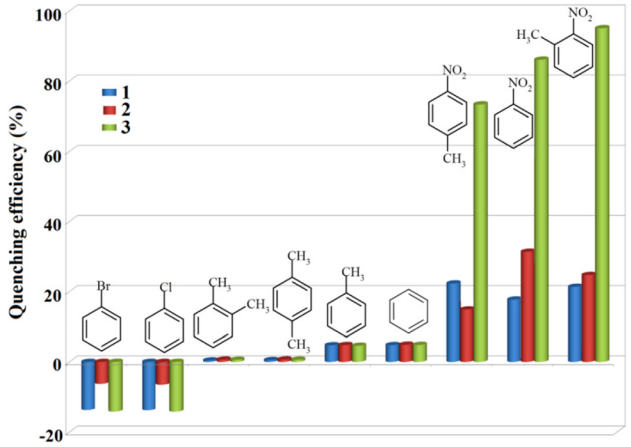

Figure 10. Quenching efficiency of fluorescence intensity at 331 nm for **1** and **2** and at 348 nm for **3.**

cies are 73.30, 86.06 and 95.05% for *p*-nitro toluene, nitro benzene and *o*-nitro toluene, respectively.

Selective fluorescence quenching behavior of **3** may be explained on the basis of photo-induced electron transfer (PET) and resonance energy transfer (RET) mechanism.[34] In PET process, electron is transferred from the excited electronic energy level of fluorophore to the LUMO of nitro aromatic compounds (NACs), a process which results in quenching of fluorescence. Hence lower the energy of LUMO of NAC, higher will be its fluorescence quenching ability. Using density functional theory (DFT) approach, we have calculated the HOMO, LUMO energies of different organic analytes. The calculated results given in Table 4S, clearly indicate that, in comparison to other analytes, the energies of LUMO of NACs of *p*-nitro toluene, nitro benzene and *o*-nitro toluene are very low and for this reason an enhanced quenching of fluorescence was observed in presence of these NACs.

On the other hand in the RET process, fluorophore undergoes excited state electron transfer process. The efficiency of fluorescence quenching in RET process depends on the extent of overlap of emission spectrum of fluorophore with the absorption spectrum of quencher. Thus higher the overlap area, higher will be the fluorescence quenching. Figures 20S, 21S and 22S show overlap of absorption spectra of NACs with emission spectrum of complexes **1, 2** and **3**, respectively. Comparison of overlap area in the spectra shows that more overlap is observed between emission spectrum of complex **3** and absorption spectra of NACs *p*-nitro toluene / nitro benzene / *o*-nitro toluene, which causes a higher quenching of fluorescence. Among these three NACs, nitrobenzene is the more electron deficient molecule, but surprisingly, the maximum fluorescence quenching of **3** is observed in the presence of *o*-nitrotoluene. This distinct behavior makes compound **3** an excellent sensor for *o*-nitrotoluene.

Figure 11 shows the change of fluorescence spectrum of compound **3** upon gradual addition of 3 μL 0.304 mM

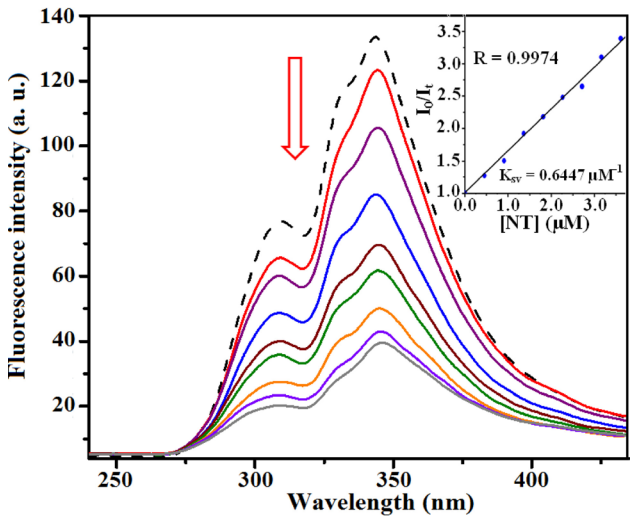

Figure 11. Fluorescence titration of **3** (2.5 ml dispersed methanolic solution) with gradual addition of 3 μL 0.304 mM methanolic solution of *o*-nitro toluene (top to bottom) at room temperature (λex = 227 nm). Inset: Stern-Volmer plot with respect to band at 348 nm.

methanolic solution of *o*-nitrotoluene. Using the Stern-Volmer equation [$I_0/I = 1 + K_{sv}$[quencher]), a linear relationship was obtained for the titration of complex **3** using *o*-nitrotoluene as quencher (Figure 11) and calculated value of binding constant was 0.644 μM^{-1}.

Conclusions

In summary we have presented here the synthesis, crystal structure, band gap calculation and fluorescence sensing behavior of three cobalt(II) complexes using N,N ′ donor neutral

ligands. Cobalt(II)–bphz in combination with linear tp and angular ip generate 1D ladder (**1**) and 2D porous (**2**) metal organic frameworks, respectively. On the other hand, a 2D interpenetrated architecture is obtained by using cobalt(II) ions and relatively long flexible connectors 1,3-bis(4-pyridyl)propane (bpp) in combination with ppda (**3**). 3D supramolecular architectures in **1–3** are realized through covalent interactions (H-bonding / $\pi\ldots\pi$ stacking). Band gap calculation reveals that all compounds act like semiconductor. Study of the effect of various organic compounds on the luminescence property of **1–3** shows that complex **3** selectively senses nitroaromatic compounds and this behavior has been explained on the basis of photo-induced electron transfer (PET) and resonance energy transfer (RET) mechanisms.

Supporting Information Summary

Experimental details, X-ray crystallographic data, IR spectra, and figures of crystal structure, electronic absorption spectra, and fluorescence spectra of complexes **1 — 3** are provided as Supporting Information.

Acknowledgements

Authors gratefully acknowledge the financial assistance given by the DST, Govt. of India, under the SERB Fast Track Scheme to Dr. Subal Chandra Manna (Grant No. SR/FT/CS-131 /2010). Authors are also thankful to Dr. Horst Puschmann (University of Durham, U.K) for crystallographic contribution of Complex 3.

Conflict of Interest

The authors declare no conflict of interest.

Keywords: Band Gap Calculation · Cobalt(II) · Dicarboxylates · Fluorescence Sensing · N-donor ligands

[1] a) O. M. Yaghi, M. O'Keeffe, N. W. Ockwig, H. K. Chae, M. Eddaoudi, J. Kim, *Nature* **2003**, *423*, 705–714; b) S. L. James, *Chem. Soc. Rev.* **2003**, *32*, 276–288; c) C. Janiak, *Dalton Trans.* **2003**, 2781–2804; d) S. Kitagawa, R. Kitaura, S. Noro, *Angew. Chem. Int. Ed.* **2004**, *43*, 2334–2375.

[2] a) D. Sun, S. Ma, Y. Ke, D. J. Collins, H. C. Zhou, *J. Am. Chem. Soc.* **2006**, *128*, 3896–3897; b) M. Eddaoudi, D. B. Moler, H. L. Li, B. L. Chen, T. M. Reineke, M. O'Keeffe, O. M. Yaghi, *Acc. Chem. Res.* **2001**, *34*, 319–330; c) G. Férey, C. Mellot-Draznieks, C. Serre, F. Millange, *Acc. Chem. Res.* **2005**, *38*, 217–225.

[3] a) M. Latroche, S. Surble, C. Serre, C. Mellot-Draznieks, P. L. Llewellyn, J. H. Lee, J. S. Chang, S. H. Jhung, G. Ferey, *Angew. Chem., Int. Ed.* **2006**, *45*, 8227–8231; b) M. H. Zeng, B. Wang, X. Y. Wang, W. X. Zhang, X. M. Chen, S. Gao, *Inorg. Chem.* **2006**, *45*, 7069–7076; c) T. Verbiest, S. van Elshocht, M. Karuanen, L. Hellemans, J. Snauwaert, C. Nuckolls, T. J. Katz, A. Persoons, *Science* **1998**, *282*, 913–915.

[4] a) P. J. Hagrman, D. Hagrman, J. Zubieta, *Angew. Chem., Int. Ed.* **1999**, *38*, 2638–2684; b) B. Chen, S. Ma, F. Zapata, F. R. Fronczek, E. B. Lobkovsky, H. C. Zhou, *Inorg. Chem.* **2007**, *46*, 1233–1236.

[5] a) B. L. Chen, N. W. Ockwig, A. R. Millward, D. S. Contreras, O. M. Yaghi, *Angew. Chem., Int. Ed.* **2005**, *44*, 4745–4749; b) B. Kesanli, W. Lin, *Coord. Chem. Rev.* **2003**, *246*, 305–326; c) S. Horike, R. Matsuda, D. Tanaka, M. Mizuno, K. Endo, S. Kitagawa, *J. Am. Chem. Soc.* **2006**, *128*, 4222–4223.

[6] a) L. F. Ma, L. Y. Wang, X. K. Huo, Y. Y. Wang, Y. T. Fan, J. G. Wang, S. H. Chen, *Cryst. Growth Des.* **2008**, *8*, 620–628; b) L. F. Ma, Y. Y. Wang, L. Y. Wang, J. Q. Liu, Y. P. Wu, J. G. Wang, Q. Z. Shi, S. M. Peng, *Eur. J. Inorg. Chem.* **2008**, 693–703.

[7] a) J. Yang, Q. Yue, G. D. Li, J. J. Cao, G. H. Li, J. S. Chen, *Inorg. Chem.* **2006**, *45*, 2857–2865; b) Q. Yue, J. Yang, G. H. Li, G. D. Li, W. Xu, J. S. Chen, S. N. Wang, *Inorg. Chem.* **2005**, *44*, 5241–5246; c) B. Q. Ma, D. S. Zhang, S. Gao, T. Z. Jin, C. H. Yan, *Angew. Chem., Int. Ed.* **2000**, *39*, 3644–3646.

[8] a) K. Hegetschweiler, B. Morgenstern, J. Zubieta, P. J. Hagrman, N. Lima, R. Sessoli, F. Totti, *Angew. Chem., Int. Ed.* **2004**, *43*, 3436–3439; b) B. Morgenstern, S. Steinhauser, K. Hegetschweiler, E. Garribba, G. Micera, D. Sanna, L. Nagy, *Inorg. Chem.* **2004**, *43*, 3116–3126;c) L. Applegarth, A. E. Goeta, J. W. Steed, *Chem. Commun.* **2005**, 2405–2406; d) S. C. Manna, J. Ribas, E. Zangrando, N. Ray Chaudhuri, *Inorg. Chim. Acta* **2007**, *360*, 2589–2597; e) S. Masaoka, D. Tanaka, Y. Nakanishi, S. Kitagawa, *Angew. Chem., Int. Ed.* **2004**, *43*, 2530–2534; f) D. Sun, Y. Ke, T. M. Mattox, B. A. Ooro, H.-C. Zhou, *Chem. Commun.* **2005**, 5447–5449.

[9] a) M. Okeeffe, M. Eddaoudi, H. Li, T. Reineke, O. M. Yaghi, *J. Solid State Chem.* **2000**, *152*, 3–20; b) M. Fujita, K. Umemoto, M. Yoshizawa, N. Fujita, T. Kusukawa, K. Biradha, *Chem. Commun.* **2001**, 509–518; c) S. R. Seidel, P. J. Stang, *Acc. Chem. Res.* **2002**, *35*, 972–983.

[10] a) S. C. Manna, K. Okamoto, E. Zangrando, N. Ray Chaudhuri, *CrystEngComm* **2007**, *9*, 199–202; b) X.-C. Huang, D. Li, X.-M. Chen, *CrystEngComm* **2006**, *8*, 351–355; c) B. Bhattacharya, D. K. Maity, P. Pachfule, E. Colacio, D. Ghoshal, *Inorg. Chem. Front.* **2014**, *1*, 414–425.

[11] A. K. Ghosh, D. Ghoshal, E. Zangrando, J. Ribas, N. Ray Chaudhuri, *Dalton Trans.* **2006**, 1554–1563.

[12] a) B. Moulton, M. J. Zaworotko, *Chem. Rev.* **2001**, *101*, 1629–1658; b) R. K. Seddon, M. J. Zaworotko, *Crystal engineering: the design and application of functional solids (NATO Science Series)*, **1999**; c) I. G. Dance, in: G. R. Desiraju, (Ed.), *The Crystals as a Supramolecular Entity, John Wiley*, NewYork, **1996**; d) D. J. Hill, M. J. Mio, R. B. Prince, T. S. Hughes, J. S. Moore, *Chem. Rev.* **2001**, *101*, 3893–4012; e) A. K. Ghosh, D. Ghoshal, T.-H. Lu, G. Mostafa, N. Ray Chaudhuri, *Cryst. Growth Des.* **2004**, *4*, 851–857; f) S. Grimme, C. Diedrich, M. Korth, *Angew. Chem., Int. Ed.* **2006**, *45*, 625–629.

[13] a) S. Mistri, E. Zangrando, A. Figuerola, A. Adhikary, S. Konar, J. Cano, S. C. Manna, *Cryst. Growth Des.* **2014**, *14*, 3276–3285; b) X. Xu, X. Zhang, X. Liu, L. Wang, E. Wang, *CrystEngComm* **2012**, *14*, 3264–3270.

[14] O. M. Yaghi, H. Li, *J. Am. Chem. Soc.* **1995**, *117*, 10401–10402.

[15] G. B. Gardner, D. Venkataraman, J. S. Moore, S. Lee, *Nature* **1995**, *374*, 792–795.

[16] a) R. W. Gable, B. F. Hoskins, R. Robson, *J. Chem. Soc., Chem. Commun.* **1990**, 1677–1678; b) M. Fujita, Y. J. Kwon, S. W. Ashizu, K. Ogura, *J. Am. Chem. Soc.* **1994**, *116*, 1151–1152; c) D. Hagrman, C. Zubieta, D. J. Rose, J. Zubieta, R. C. Haushalter, *Angew. Chem., Int. Ed. Engl.* **1997**, *36*, 873–878.

[17] a) F. Robinson, M. J. Zaworotko, *J. Chem. Soc., Chem. Commun.* **1995**, 2413–2414; b) O. M. Yaghi, H. Li, *J. Am. Chem. Soc.* **1996**, *118*, 295–296.

[18] a) M. Fujita, Y. J. Kwon, Y. O. Sasaki, K. Yamaguchi, K. Ogura, *J. Am. Chem. Soc.* **1995**, *117*, 7287–7288; b) P. Losier, M. J. Zaworotko, *Angew. Chem., Int. Ed. Engl.* **1996**, *35*, 2779–2782; c) T. L. Hennigar, D. C. MacQuarrie, P. Losier, R. D. Rogers, M. J. Zaworotko, *Angew. Chem., Int. Ed. Engl.* **1997**, *36*, 972–973.

[19] S. R. Batten, R. Robson, *Angew. Chem. Int. Ed.* **1998**, *37*, 1460–1494.

[20] a) S. C. Manna, S. Konar, E. Zangrando, K.-I. Okamoto, J. Ribas, N. Ray Chaudhuri, *Eur. J. Inorg. Chem.* **2005**, 4646–4654; b) S. C. Manna, A. D. Jana, G. M. Rosair, M. G. B. Drew, G. Mostafa, N. Ray Chaudhuri, *J. Solid State Chem.* **2008**, *181*, 457–466.

[21] a) http://www.chem.monash.edu.au/staff/sbatten/index.html, and references therein; b) L. Carlucci, G. Ciani, D. M. Proserpio, S. Rizzato, *Chem. -Eur. J.* **2002**, *8*, 1519–1526; c) P. Metrangolo, F. Meyer, T. Pilati, D. M. Proserpio, G. Resnati, *Chem.-Eur. J.* **2007**, *13*, 5765–5772; d) Y.-F. Hsu, C.-H. Lin, J.-D. Chen, J.-C. Wang, *Cryst. Growth Des.* **2008**, *8*, 1094–1096.

[22] a) E. G. Bakalbassis, M. Korabik, A. Michailides, J. Mrozinski, C. Raptopoulou, S. Skoulika, A. Terzis, D. Tsaousis, *J. Chem. Soc., Dalton Trans.* **2001**, 850–857; b) C. Livage, C. Egger, M. Nogues, G. Férey, *J. Mater. Chem.* **1998**, *8*, 2743–2747; c) C. Livage, C. Egger, G. Férey, *Chem. Mater.* **1999**, *11*, 1546–1550; d) L. Deakin, A. M. Ariff, J. S. Miller, *Inorg. Chem.* **1999**, *38*, 5072–5077; e) M.-F. S. Lo, S.-Y. S. Chui, I. D. Willams, L. Y. Shek, Z. Lin, X. X. Zang, G. H. Wen, *J. Am. Chem. Soc.* **2000**, *122*, 6293–6294.

[23] a) S. C. Manna, S. Mistri, A. D. Jana, *CrystEngComm* **2012**, *14*, 7415–7422; b) S. Mistri, E. Zangrando, S. C. Manna, *Inorg. Chim. Acta* **2013**, *405*, 331–338; c) S. C. Manna, E. Zangrando, J. Ribas, N. Ray Chaudhuri, *Eur. J.*

Inorg. Chem. **2007**, 4592–4595; d) S. Konar, S. C. Manna, E. Zangrando, T. Mallah, J. Ribas, N. Ray Chaudhuri, *Eur. J. Inorg. Chem.* **2004**, 4202–4208; e) S. C. Manna, E. Zangrando, M. G. B. Drew, J. Ribas, N. Ray Chaudhuri, *Eur. J. Inorg. Chem.* **2006**, 481–488; f) S. C. Manna, E. Zangrando, A. Bencini, C. Benelli, N. RayChaudhuri, *Inorg. Chem.* **2006**, *45*, 9114–9122.

[24] a) C. Livage, N. Guillou, J. Chaigneau, P. Rabu, M. Drillon, G. Férey, *Angew. Chem. Int. Ed.* **2005**, *44*, 6488–6491; b) B. Bhattacharya, D. K. Maity, R. Mondal, E. Colacio, D. Ghoshal, *Cryst. Growth Des.* **2015**, *15*, 4427–4437.

[25] S. C. Manna, E. Zangrando, J. Ribas, N. Ray Chaudhuri, *Dalton Trans.* **2007**, 1383–1391.

[26] a) J. P. Desvergne, A. W. Czarnik (Eds.), *Chemosensors of Ion and Molecule Recognition*, Kluwer Academic Publishers, Boston, **1997**; b) A. P. de Silva, H. Q. N. Gunaratne, T. Gunnlaugsson, A. J. M. Huxley, C. P. McCoy, J. T. Rademacher, T. E. Rice, *Chem. Rev.* **1997**, *97*, 1515–1566.

[27] a) B. Gole, A. K. Bar, P. S. Mukherjee, *Chem. Commun.* **2011**, *47*, 12137–12139; b) Z. Zhang, S. Xiang, X. Rao, Q. Zheng, F. R. Fronczek, G. Qian, B. Chen, *Chem. Commun.* **2010**, *46*, 7205–7207; c) C. Zhang, Y. Che, Z. Zhang, X. Yang, L. Zang, *Chem. Commun.* **2011**, *47*, 2336–2338; d) S. Pramanick, C. Zheng, X. Zhang, T. J. Emge, J. Li, *J. Am. Chem. Soc.* **2011**, *133*, 4153–4155; e) S. Mistri, E. Zangrando, S. C. Manna, *Polyhedron* **2013**, *49*, 252–258.

[28] a) K. Nakamoto, Infrared Spectra of Inorganic and Coordination Compounds, John Wiley & Sons, New York, (**1997**); b) V. Zelenak, Z. Vargova, K. Gyoryova, *Spectrochimica Acta Part A* **2007**, *66*, 262–272; c) G. B. Deacon, R. J. Phillip, *Coord. Chem. Rev.* 1980, 33, 227–250; d) W. Lewandowski, M. Kalinowska, H. Lewandowska, *J. Inorg. Biochem.* 2005, 99, 1407–1423.

[29] S. R. Batten, *CrystEngComm* **2001**, *3*, 67–72.

[30] L. Carlucci, G. Ciani, D. M. Proserpio, S. Rizzato, *CrystEngComm* **2002**, *4*, 121–129.

[31] a) V. Vajpayee, S. Lee, S.-H. Kim, S. C. Kang, T. R. Cook, H. Kim, D. W. Kim, S. Verma, M. S. Lah, I. S. Kim, M. Wang, P. J. Stang, K.-W. Chi, *Dalton Trans.* **2013**, *42*, 466–475; b) M. De-Yun, Q. Liang, G. Hai-Fu, L. Huang, *Chinese J. Inorg. Chem.* **2013**, *29*, 1–6; c) F. Bardak, C. Karaca, S. Bilgili, A. Atac, T. Mavis, A. M. Asiri, M. Karabacake, E. Kose, *Spectrochimica Acta Part A: Molecular and Biomolecular Spectroscopy* **2016**, *165*, 33–46; d) K. Faghihi, *Turk J Chem.* **2008**, *32*, 191–200; e) N. Karthikeyan, J. J. Prince, S. Ramalingam, S. Periandy, *Spectrochimica Acta Part A: Molecular and Biomolecular Spectroscopy http://dx.doi.org/10.1016/j.saa.2014.11.112.*

[32] a) M. Che, J. C. Vedrine, Characterization of Solid Materials and Heterogeneous Catalysts, John Wiley & Sons, Germany, (**2012**); b) R. Ghosh, A. F. Pedicini, P. C. Rao, K. S. Asha, A. C. Reber, S. Mandal, *Dalton Trans.* **2015**, *44*, 13464–13468; c) J.-N. Rebilly, P. W. Gardner, G. R. Darling, J. Bacsa, M. J. Rosseinsky, *Inorg. Chem.* **2008**, *47*, 9390–9399.

[33] a) H. Zhao, C. Zhang, *J. Inorg. Organomet. Polym.* **2015**, *25*, 912–920; b) Y. V. Kokunov, Y. E. Gorbunova, V. V. Kovalev, A. S. Kozyukhin, *Russian J. Inorg. Chem.* **2014**, *59*, 187–191.

[34] S. S. Nagarkar, A. V. Desaia, S. K. Ghosh, *CrystEngComm* **2016**, *18*, 2994–3007.

Submitted: February 6, 2017
Accepted: March 6, 2017